Advances in Atmospheric Sciences
Impact Factor: 3.158
E-alert
ISSN 0256-1530
CN 11-1925/O4

Distinguishing the Regional Atmospheric Controls on Precipitation Isotopic Variability in the Central–Southeast Portion of Brazil

Vinícius dos SANTOS, Peter MARSHALL FLEMING, Luís HENRIQUE MANCINI, Stela DALVA SANTOS COTA, Graziele Beatriz de LIMA, Rafaela RODRIGUES GOMES, Roberto Eduardo KIRCHHEIM, Ricardo SANCHZ–MURILLO, Didier GASTMANS

Citation: dos Santos, V., and Coauthors 2022: Distinguishing the Regional Atmospheric Controls on Precipitation Isotopic Variability in the Central–Southeast Portion of Brazil, *Adv. Atmos. Sci.*, In press. doi: 10.1007/s00376–022–1367–0.

View online: https://doi.org/10.1007/s00376–022–1367–0

ADVANCES IN ATMOSPHERIC SCIENCES, VOL. 39, OCTOBER 2022, 1693–1708

• Original Paper •

Distinguishing the Regional Atmospheric Controls on Precipitation Isotopic Variability in the Central-Southeast Portion of Brazil

Vinícius dos SANTOS[1], Peter MARSHALL FLEMING[2], Luís HENRIQUE MANCINI[3], Stela DALVA SANTOS COTA[2], Graziele Beatriz de LIMA[1], Rafaela RODRIGUES GOMES[1], Roberto Eduardo KIRCHHEIM[4], Ricardo SANCHÉZ-MURILLO[5,6], and Didier GASTMANS[*1]

[1]*São Paulo State University* (*UNESP*), *Environmental Studies Center*. *Av*. 24*ABased*, 1515 – *Bela Vista*, 13.506-900, *Rio Claro* (*SP*), *Brazil*

[2]*Center for the Development of the Nuclear Technology* (*CDTN – CNEN*), *Av. Presidente Antônio Carlos*, 6.627, *Campus da UFMG – Pampulha*, 31270-90, *Belo Horizonte* (*MG*), *Brazil*

[3]*Universidade de Brasília – UnB*, *Instituto de Geociências, Laboratório de Isótopos Estáveis*. *Campus "Darcy Ribeiro"*, *Asa Norte*, 70.910-900, *Brasília* (*DF*), *Brasil*

[4]*Hydrology and Territorial Management Directory (DHT)*, *The Geological Survey of Brazil (CPRM-SGB)*, *São Paulo (SP)*, *Brazil*

[5]*University of Texas at Arlington*, *Earth and Environmental Sciences Department*, 500 *Yates Street*, *Arlington*, *Texas*, 76019, *USA*

[6]*Stable Isotopes Research Group and Water Resources Management Laboratory*, *Universidad Nacional*, *Heredia*, *Costa Rica*

(Received 15 September 2021; revised 20 January 2022; accepted 15 February 2022)

ABSTRACT

Precipitation isotope ratios (O and H) record the history of water phase transitions and fractionation processes during moisture transport and rainfall formation. Here, we evaluated the isotopic composition of precipitation over the central-southeastern region of Brazil at different timescales. Monthly isotopic compositions were associated with classical effects (rainfall amount, seasonality, and continentality), demonstrating the importance of vapor recirculation processes and different regional atmospheric systems (South American Convergence Zone-SACZ and Cold Fronts-CF). While moisture recycling and regional atmospheric processes may also be observed on a daily timescale, classical effects such as the amount effect were not strongly correlated (δ^{18}O-precipitation rate $r \leqslant -0.37$). Daily variability revealed specific climatic features, such as δ^{18}O depleted values (~ –6‰ to –8‰) during the wet season were associated with strong convective activity and large moisture availability. Daily isotopic analysis revealed the role of different moisture sources and transport effects. Isotope ratios combined with *d*-excess explain how atmospheric recirculation processes interact with convective activity during rainfall formation processes. Our findings provide a new understanding of rainfall sampling timescales and highlight the importance of water isotopes to decipher key hydrometeorological processes in a complex spatial and temporal context in central-southeastern Brazil.

Key words: precipitation, stable water isotopes, *d*-excess, moisture source and transport, southern Atlantic Ocean and Amazon

Citation: dos Santos, V., and Coauthors, 2022: Distinguishing the regional atmospheric controls on precipitation isotopic variability in the central-southeast portion of Brazil. *Adv. Atmos. Sci.*, **39**(10), 1693−1708, https://doi.org/10.1007/s00376-022-1367-0.

Article Highlights:

- A significant correlation was observed between monthly precipitation amounts and δ^{18}O values ($r \geqslant 0.60$).
- Strong daily δ^{18}O correlations ($r \geqslant 0.50$) were associated with regional meteorological features such as OLR.
- Air mass back trajectories and *d*-excess values (>13‰) showed the role of the Amazon Forest on moisture recirculation and availability.
- Our results indicate the major importance of convection activity ($r = 0.65$ – δ^{18}O-OLR) and moisture availability ($r = –0.66$ – δ^{18}O-Precipitable Water) controlling rainfall generation and the isotopic variability.

* Corresponding author: Didier GASTMANS
Email: didier.gastmans@unesp.br

1. Introduction

The stable water isotopologues constitute an important tool to underpin the climatic controls involved in rainfall formation processes, considered one of the most vulnerable components of the hydrological cycle under a changing climate (Power et al., 2017; Wasko and Sharma, 2017). Different isotopologues are formed due to the isotopic fractionation during aqueous phase changes. Therefore, it is possible to trace and combine their isotopic compositions with physical and microphysical processes within distinct water reservoirs at the surface-atmosphere continuum (Bowen et al., 2019).

Since the establishment of the Global Network of Isotopes in Precipitation in 1961 (known as GNIP; https://www.iaea.org/services/networks/gnip), multiple efforts have addressed the key climatic drivers governing the isotopic composition of precipitation (Rozanski et al., 1993; Clark and Fritz, 1997; Aggarwal et al., 2012; Terzer et al., 2013; Konecky et al., 2019). However, the isotopic drivers are still not well defined in tropical areas, whereby weak correlations with temperature and moderate negative correlations with the amount of precipitation (known as the "amount effect") (Dansgaard, 1964; Kurita et al., 2009; Winnick et al., 2014; Sánchez-Murillo et al., 2016) are the most recurrent findings. Recently, convective and stratiform precipitation processes (Risi et al., 2008; Aggarwal et al., 2016; Tharammal et al., 2017; Lekshmy et al., 2018; Munksgaard et al., 2019; Sánchez-Murillo et al., 2019) have been considered to be the main factor that explains precipitation isotopic variability in the tropics and a large portion of extratropical areas worldwide (Aggarwal et al., 2016). However, the linear regression model used for rainfall correlation has already been debated (Konecky et al., 2019) since the humidity convergence processes and rain re-evaporation were not considered.

The combination of more robust analytical instrumentation and techniques combined with the greater efficiency of reliable precipitation passive collectors (Michelsen et al., 2018, 2019) allow for the exploration of precipitation processes at different timescales (i.e., monthly, weekly, daily, and intra-events). Kurita et al. (2009) demonstrated that daily isotopic compositions reflect: 1) the regional atmospheric conditions (i.e., moisture source, rain-out history during transport) such as on a monthly timescale; 2) local effects (i.e., topography, surface meteorological conditions); and 3) post-condensation processes (i.e., the interaction between raindrops and the surrounding water vapor under the cloud and/or re-evaporation during the raindrops descent). It is necessary to emphasize that in daily or subdaily monitoring strategies, the correlation between $\delta^{18}O$ and the rain intensity (recognized as the amount effect) tends to be weak (Kurita et al., 2009). This lack of correlation on daily basis (or amount effect) was directly related to regional factors, such as air mass origin, its trajectory, and the precipitation history or local factors (below-cloud processes, which depend on rain intensity, relative humidity, and drop sizes). During intense rainfall events, drops tend to be larger and hence less affected by isotopic exchanges with vapor (Muller et al., 2015; Graf et al., 2019; Han et al., 2020, 2021).

Our study combines the isotopic compositions of monthly and daily precipitation data, collected over different timescales and obtained from meteorological stations located in the central-southeastern region of Brazil: Belo Horizonte-MG, Brasília-DF, Rio Claro-SP, and Rio de Janeiro-RJ, hereafter BH, BR, RC, and RJ, respectively (Fig. 1 and Table 1). This region is characterized by a high population density and high concentrations of large industrial and agro-industrial activities; therefore, sustaining water resources is one of the main challenges for managers and government agencies (Ferreira et al., 2018). Belo Horizonte, Brasília, and Rio de Janeiro are socio-climatic hot spots (Torres et al., 2012), while Rio Claro is located in the Parana Basin, close to important recharge areas of the Guarani Aquifer System (Batista et al., 2018; Kirchheim et al., 2019; Santarosa et al., 2021).

The main objective of this study is to evaluate the multitemporal rainfall isotopic variability over the central-southeastern region of Brazil and identify how distinct isotope sampling timescales enhance our understanding of key drivers controlling rainfall generation. The main research questions are 1) How do different climatic regimes/conditions affect the isotopic composition at each location on monthly and daily sampling scales? 2) Do the atmospheric systems promote the same influence over isotopic variability at all stations? 3) Does changing the sampling timescale, monthly or daily, affect the insights for isotopic interpretation in tropical areas?

Our results offer an enhanced isotopic assessment of tropical rain, provide novel information and knowledge to improve the current regional and global interpretations of stable isotope variations in tropical rainfall under climate change scenarios. Furthermore, this study promotes an interpretation of new data using two timescales in a large regional area. From this perspective, the study of the isotopic composition of precipitation in Brazil represents a research area that has received limited attention.

The remainder of this paper is organized as follows. Section 2 discusses the background settings, section 3 outlines the materials and methods with isotopes analysis and meteorological data, section 4 presents the results in two parts, from monthly to daily timescales, section 5 discusses the results, and section 6 presents the conclusions from this research.

2. General settings

The rainfall pattern in central-southeastern Brazil is characterized by an annual average of around 1500 mm and is divided into two distinct seasons, the dry season (April to September) and the wet season (October to March) (Reboita et al., 2010; Alvares et al., 2013). Recycled moisture (i.e., evapotranspiration) from the Amazon rainforest is the main water vapor source during the wet season (Fig. 1). Amazon moisture is transported by the Low-Level Jet (LLJ), providing

moisture flux from the east of the Andes range (i.e., Amazon region) to the southeast region of South America (Marengo et al., 2004; Montini et al., 2019; Ramos et al., 2019). The interactions between the incursions of Bolivian High (BoH), LLJ, and Cold Fronts (CF) on the southeastern coast contribute to the formation of the South American Convergence Zone (SACZ), an area of enhanced convective activity with a wide range of cloud coverage, humidity, and heavy rainfall during the Brazilian summer (Kodama, 1992; Lima et al., 2010) (Fig.1). These climatic features are all part of the seasonal dynamic of the South America Summer Monsoon system (Vera et al., 2006; Reboita et al., 2010; Marengo et al., 2012). During the dry season, there is decreased moisture flux into the Amazon, a displacement of the southern Atlantic Subtropical High (SASH) over the continent, and, consequently, a decrease in rainfall due to strong CF incursions (Reboita et al., 2010).

3. Materials and methods

3.1. *Isotopic composition of monthly and daily precipitation*

Monthly isotopic compositions at BH, BR, and RJ were obtained from the GNIP dataset (reference code in Table 1, available at: https://www.iaea.org/services/networks/gnip). Both monthly and daily samples were collected in RC at the Environmental Studies Center – São Paulo State University (CEA-UNESP) and were analyzed using Cavity Ring-Down Laser Spectroscopy at the Hydrogeology and Hydrochemistry laboratory of UNESP's Department of Applied Geology, according to dos Santos et al. (2019c), available at https://data.mendeley.com/datasets/72z5cyhg9g/1. The BR daily isotopic composition was collected at the Laboratory of the Geochronological, Geodynamics and Environmental Studies - Brasília University (UnB). The samples were analyzed at the Laboratory of the Stable Isotopes using a Picarro L2120-i Analyzer - Vaporization Module A0211 and Autosampler PAL HTC-xt. The BH daily samples were collected and analyzed at the Center for the Development of the Nuclear Technology (CDTN) using a Delta V IRMS Thermo Fischer system, model Delta V Advantage Isotope Ratio MS.

3.2. *Meteorological data and El Niño-southern Oscillation (ENSO) analysis*

Precipitation, temperature, and relative humidity surface data from BH (OMM code: 83587, 19.93°S, 43.93°W), BR (OMM code: 83377, 15.78°S, 47.92°W), and RJ (OMM Code: 83743, 22.89°S, 43.18°W) were obtained from the Meteorological Dataset for Education and Research (BDMEP) at the National Institute of Meteorology (INMET), available at: http://www.inmet.gov.br/portal/

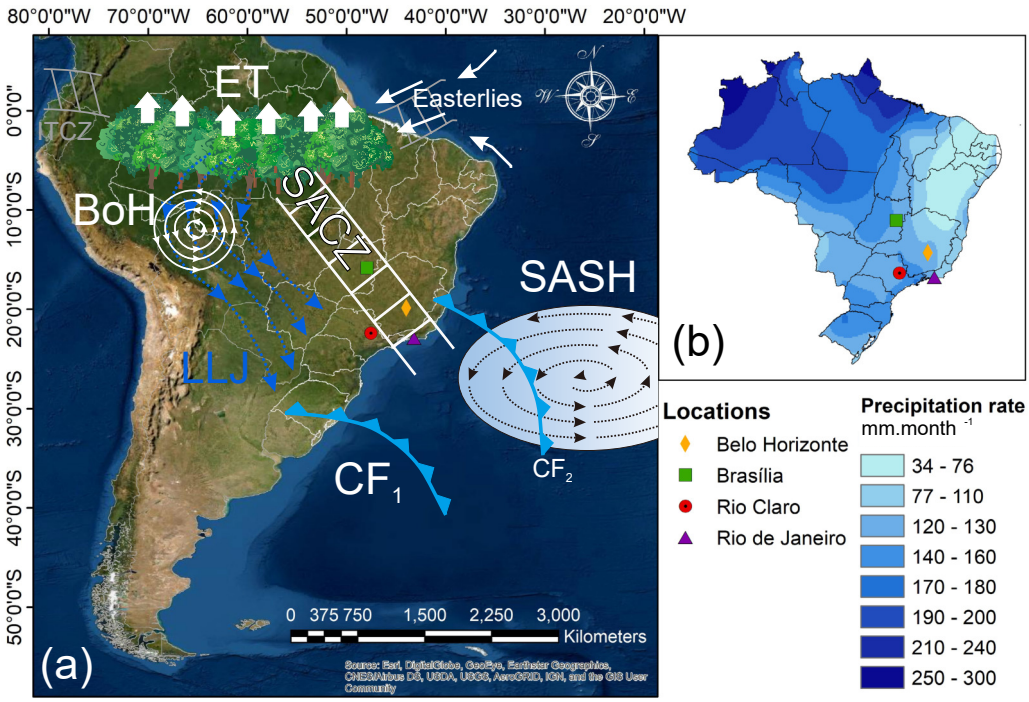

Fig. 1. Circulation patterns and atmospheric systems: (a) ET: Evapotranspiration; ITCZ: Intertropical Convergence Zone; BoH: Bolivian High; LLJ: Low-Level Jet; SACZ: South America Convergence Zone; SASH: southern Atlantic Subtropical High; CF: Cold Front (CF1 = of extratropical origin; CF2 = associated with the formation of SACZ). Figure based on Marengo et al. (2004) and modified from Santos et al. (2019a); (b) Stable isotope sampling locations. Annual precipitation (color-coded in mm) was obtained from the dataset of the Climate Prediction Center Merged Analysis of Precipitation, available at: http://www.cpc.ncep.noaa.gov/products/global_precip/html/wpage.cmap.html.

index.php?r=bdmep/bdmep. Surface meteorological data for RC were obtained from a meteorological station located at the Centro de Análise e Planejamento Ambiental—São Paulo State University Rio Claro (22°23′S, 47°32′W). Historical precipitation data ranges are 1961 to 2018 (BH), 1965 to 2018 (BR), 1994 to 2018 (RC), and 1961 to 1983/2002 to 2016 (RJ).

The influence of ENSO in the study area was assessed using the Oceanic Niño Index (ONI), which identifies different ENSO phases and classifies each intensity based on a continuous average of sea surface temperature anomalies (TSM) of three months in the Niño region 3.4. over the Pacific Ocean (5°N–5°S, 120°–170°W) (Huang et al., 2017). According to the National Oceanic and Atmospheric Administration (NOAA) (http://origin.cpc.ncep.noaa.gov/products/analysis_monitoring/ensostuff/ONI_v5.php), an ENSO event is defined as SST values exceeding a threshold of ±0.5°C for a minimum of five consecutive overlapping months. Positive and negative anomalies are defined as La Niña (cold phase) and El Niño (warm phase), respectively.

Due to different periods covered by the isotopic data (Table 1), locations were separated to compare ENSO events during the same period. At stations BR and RJ, the following ENSO events were selected: 1) warm phase: March 1965–April 1966 and October 1968–December 1969; and 2) cold phase: May 1973–June 1974, October 1974–April 1976). At BH and RC, the following ENSO events were selected: 1) warm phase: November 2014–May 2016; and 2) cold phase: August–December 2016 and October 2017–March 2018. A regression analysis was carried out for these ENSO events, including the monthly isotopic compositions and the ONI-Index. Historical precipitation values were used to determine the standard precipitation anomaly during ENSO phases. At the RC station, the precipitation data (1950–2016) were obtained from dos Santos et al. (2019b) and were updated to include 2017 and 2018.

3.3. *HYSPLIT and synoptic analysis*

The origin of the air masses, their trajectories, and the subsequent precipitation for the daily isotopic composition at BH, BR, and RC were analyzed using the HYSPLIT model (Hybrid Single-Particle Lagrangian Integrated Trajectory) (Stein et al., 2015; Rolph et al., 2017). This model uses a 3D Lagrangian air mass vertical velocity algorithm to determine the position of the air masses and reports these values at hourly time resolution over the trajectory (Soderberg et al., 2013; Sánchez-Murillo et al., 2017). The trajectories of the air masses were estimated for 240 hours prior to precipitation onset, considering the estimated time of residence of the water vapor (Gimeno et al., 2010; van der Ent and Tuinenburg, 2017; Gimeno et al., 2021). The trajectories were computed using NOAA′s meteorological data (global data assimilation system, GDAS: 1 degree, global, 2006-present), with ending elevations of the trajectories at 1500 m above the surface, taking into account the climatological height of the LLJ, within 1000–2000 m (Marengo et al., 2004). The HYSPLIT model also calculates meteorological outputs along the trajectories, such as ambient temperature (K), relative humidity (RH%), rainfall intensity (mm hr^{-1}), and mixed layer depth (mix depth m). The mixing depth is calculated based on the potential temperature profile (Draxler et al., 2020) Trajectory frequency maps were generated as the sum of the number of times the trajectories passed through one 3° grid cell using ArcGIS software.

The synoptic atmosphere analysis was carried out based on the NCEP/NCAR (National Center for Environmental Prediction/National Center for Atmospheric Research) reanalysis of data from the National Oceanic and Atmospheric Administration – NOAA (Kalnay et al., 1996) (https://psl.noaa.gov/data/composites/day/). This dataset was used to generate plots of vertically integrated precipitable water (kg m^{-2}) and the 500 hPa vertical velocity field or Omega (Pa s^{-1}) with grid size 2.5° × 2.5°, and Outgoing Longwave Radiation (OLR W m^{-2}), grid size 1.0° × 1.0°.

The OLR is a thermal radiative flux emitted by the earth's surface and was used as an indicator for the convective activity (Vuille and Werner, 2005), since values below 240 W m^{-2} indicate organized deep convection, while values above 240 W m^{-2} suggest no organized convection occurrence (Gadgil, 2003). The positive and negative Omega corresponded to downward and upward motion (convective activity), respectively.

3.4. *Convective and stratiform precipitation by ERA-Interim*

The ERA-Interim is a global atmosphere reanalysis from the European Centre for Medium-Range Weather Forecasts (ECMRWF). This model and reanalysis system uses ECMWF's Integrated Forecast System (IFS-31r2), configured for the following spatial resolution: 60 levels in the verti-

Table 1. General information of precipitation sampling locations.

Location	GNIP Code	Latitude	Longitude	Elevation. (m)	Timescale	*n*	Period	Climate Type
Belo Horizonte	8358301	19.87°S	43.96°W	857	Monthly	91	10/2008-12/2018	Cwb
					Daily	43	09/2016-02/2017	
Brasilia	8337800	15.85°S	47.93°W	1061	Monthly	115	03/1965-06/1987	Aw
		15.76°S	47.89°W	1071	Daily	75	09/2016-03/2017	
Rio Claro	8374701	22.39°S	47.54°W	670	Monthly	65	02/2013-12/2018	Cwa
					Daily	69	09/2016-03/2017	
Rio de Janeiro	8374300	22.90°S	43.17°W	29	Monthly	131	11/1961-09/1985	Aw

Elev. = elevation in meters; *n* = number of samples; Climate type based on Koppen's climate classification map for Brazil by Alvares et al. (2013).

cal, with the top level at 0.1 hPa, T255 spherical-harmonic representation for the basic dynamical fields, and a reduced Gaussian grid with approximately uniform 79 km spacing for the surface and other grid-point fields (Berrisford et al., 2011). The ERA-Interim provides daily convective and large-scale precipitation (stratiform), with 3-hr resolution and a spatial resolution grid of 0.75° × 0.75°.

The convective and large-scale (stratiform) precipitation data were obtained online (https://apps.ecmwf.int/datasets/data/interim-full-daily/levtype=sfc/). Every grid pixel represents the amount of convective and large-scale precipitation [m of water and was converted to millimeters (mm)] based on the prognostic parameterization of cloud schemes by ECMWF (de Leeuw et al., 2015). Data were obtained for spatial grids corresponding to the BH, BR, and RC stations (Table 1), according to local precipitation intervals recorded by the meteorological stations, which correspond to cumulative precipitation samples from the previous day at 1200 UTC to the next day at 1200 UTC (equivalent to 24 houyrs). In the partitioning of ECMWF scheme by ERA-interim, the large-scale precipitation is considered stratiform precipitation (de Leeuw et al., 2015).

3.5. *Statistical Analysis*

A Kruskal-Wallis (Kruskal and Wallis, 1952) nonparametric test was applied to test statistical differences (p-value < 0.05) between the isotopic compositions ($\delta^{18}O$, $\delta^{2}H$ and d-excess) for each locality. The D'Agostino-Pearson K^2 statistic ($n \geq 20$ and k samples) (D'Agostino et al., 1990) was applied to verify that the data distribution was normal (parametric) or non-normal (non-parametric). A significant difference (p-value < 0.05) indicates a nonparametric distribution. A Spearman correlation test was used for nonparametric distribution data, whereas Pearson's linear correlation test was applied for parametric data. These statistical tests (analysis of variance, normality, and correlation) were conducted between monthly and daily isotope ratios ($\delta^{18}O$, $\delta^{2}H$, and d-excess) and meteorological data (i.e., local station data, ONI-Index, HYSPLIT model, and rainfall type from the ERA-Interim). All tests were performed with significance levels defined by a p-value (p) < 0.05, using the Corrplot R package (R Core Team, 2020).

4. Results

4.1. *Climatic patterns and precipitation*

During the monitoring period (Table 1), the average monthly precipitation (AMPrecip) in all sites presented evident seasonal distributions, following the pattern observed in long-term monthly precipitation (Fig. 2). In terms of the AMPrecip values, December was the rainiest month at BH (275 mm) and BR (236 mm), while at RJ and RC, January featured greater values, at 207 and 204 mm, respectively. In contrast, July was the driest month at RC (18 mm), June in BR (19 mm), June and August in BR (30 mm), and August in RJ (41 mm) (Fig. 2). The wet season represents the largest contribution for annual precipitation, ranging from 83% in BH, 79% in BR, 71% in RC, and 68% in RJ.

The influence of ENSO on precipitation was determined based on the long-term monthly precipitation (1960–2018) for all sites. Weak annual precipitation anomalies were found during both phases. During the warm phase, rainfall increases were reported in RC (12.6%), RJ (2.5%), and BR (1.9%), and a decrease was noted at BH (–5.6%). During the cold phase, the net rainfall anomalies were as smaller in all sites, with decreases at BH (–5.8%), RC (–1.4%), BR (–0.3%), and a small increase at RJ (0.1%) (Fig. S1 in the Electronic Supplementary Materials, ESM).

Temperature also presented a seasonal pattern. The difference between the hottest monthly average, January for BH (21°C), RC (24°C), and RJ (26°C), and the coldest monthly average did not exceed 7°C in RC and BH, while at RJ and BR seasonal average temperature only differed by 5°C and

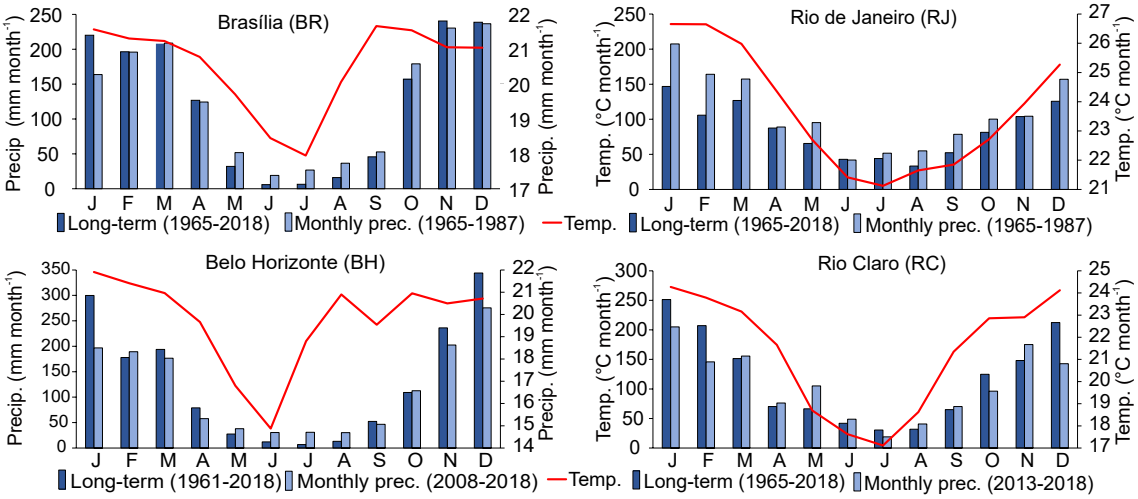

Fig. 2. Monthly averages of meteorological data in Central-Southeast of Brazil. Long-term monthly precipitation (left bars) versus arithmetic mean monthly precipitation records during the isotope sampling period (right bars). The red line is the arithmetic mean temperature during the isotope monitoring period.

3°C, respectively (Fig. S2 in the ESM).

4.2. *Monthly and seasonal isotopic variability*

Differences in the average monthly isotopic composition ($\delta^{18}O$ and $\delta^{2}H$) are presented in Figs. 3a–b. Overall, $\delta^{18}O$ mean values were: –4.91‰ (BH), –4.58‰ (RC), –4.08‰ (BR), and –3.72‰ (RJ). The BR station presented higher isotopic variability, while a lower variation was observed at

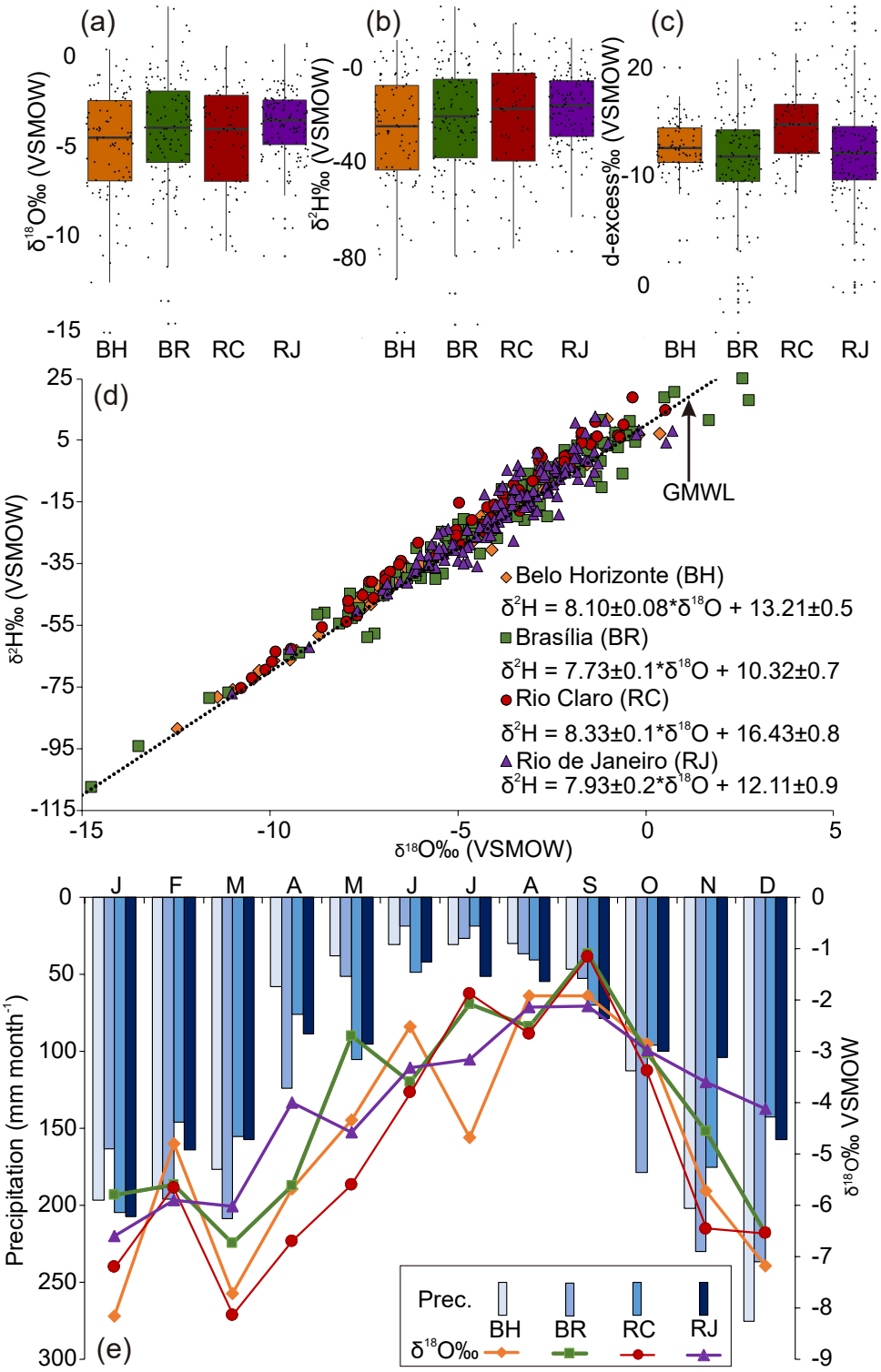

Fig. 3. Monthly isotopic compositions of precipitation at each site: (a) $\delta^{18}O$, (b) $\delta^{2}H$, and (c) *d*-excess dispersion boxplots; (d) Dual $\delta^{18}O$ and $\delta^{2}H$ plot including the Global Meteoric Water Line (GMWL) for reference and Local Meteoric Water Lines (LMWLs) regressions; (e) monthly average precipitation in bars, and weighted mean isotopes given by lines.

BH, RC, and RJ. As expected, δ^2H values exhibited a similar distribution. Differences were also observed for *d*-excess (Fig. 3c). Greater *d*-excess values were observed at RC and RJ sites (*d*-excess > 12‰), while BR reported lower *d*-excess values. Amount-weighted $\delta^{18}O$ averages were lower than the arithmetic $\delta^{18}O$ means for all sites, ranging from –6.25‰ in BH, –5.07‰ in BR, –4.87‰ in RC, and RJ (–2.64‰). Isotope values were plotted along to the Global Meteoric Water Line (GMWL), with the slope of Local Meteoric Water Lines (LMWLs) close to 8 and intercepts greater than 11 for RJ, BH, and RC sites, except for BR that had an intercept near 10‰ (Fig. 3d).

On a seasonal basis, the isotopic compositions exhibited depleted values during the wet season and enriched values during the dry season, with the most depleted $\delta^{18}O$ values occurring during January, March, and December (~ –6‰ to –8‰) and enriched values observed from July to September (~ –4‰ to –1‰). Despite the similarity of the seasonal distributions, the Kruskal-Wallis test revealed statistically significant monthly differences between the sites for $\delta^{18}O$ (p = 0.03) and *d*-excess (p = < –0.0001) (Fig. 3e). For δ^2H, no significant statistical differences were observed.

Overall, significant negative correlations between the amount of precipitation and $\delta^{18}O$ values were observed across all sites (Table 2). Relationships between the isotopic values and temperature (except in RJ; Table 2) exhibited weak correlations. Elevation and latitudinal effects were also not observed. The most depleted values were recorded at the BH station (857 m elevation). Despite the moderate and positive correlation between the isotopic composition and the ONI-Index during the cold phase of ENSO at BH and RC (Table 2), the *p*-value is not significant (> 0.05 for all localities). For δ^2H and *d*-excess, the correlations with meteorological parameters are not strong, except for δ^2H-temperature (Table 2).

4.3. *Daily isotopic variability*

The assessment of the daily isotopic composition at BH (September 2016–February 2017), BR, and RC (September 2016–March 2017) indicates relatively small differences as demonstrated by the amplitudes (Figs. 4a–c) and the average $\delta^{18}O$ values: –4.03‰±3.72‰ (BH), –3.39‰±3.88‰ (BR) and –4.85‰±4.34‰ (RC). Isotopic composition at RC was the most depleted during this period (Figs. 4a and b), while greater *d*-excess values were observed at BR (Fig. 4c). The Kruskal-Wallis test indicated a statistically significant difference for *d*-excess among all sites, while for $\delta^{18}O$ and δ^2H, no significant differences were observed.

Computed daily LMWLs presented similar slopes and intercepts: BH ($\delta^2H = 7.79 \pm 0.16\delta^{18}O + 10.74 \pm 0.89$); BR ($\delta^2H = 7.42 \pm 0.12\delta^{18}O + 12.68 \pm 0.64$); RC ($\delta^2H = 7.96 \pm 0.12\delta^{18}O + 12.93 \pm 0.80$).

The temporal distribution of the isotopic composition of precipitation is different between locations (Fig. 4). At BH (Fig. 4d) and BR (Fig. 4e), $\delta^{18}O$ exhibited two depleted incursions (October–November and February–March). Strong depletions were observed at BR during February 2017. At RC, moderate depletions were observed until late December, with strong incursions between January and March (Fig. 4f). In general, low $\delta^{18}O$ values were observed during months with larger precipitation amounts (Fig. 4). Most portions of rain events were characterized by a greater convective precipitation-ERA (Cv) fraction (Fig. S3 in the ESM); however, the Cv and Stratiform (St) precipitation of the ERA does not correlate with $\delta^{18}O$-δ^2H values.

Greater $\delta^{18}O$-δ^2H correlations ($r \geq 0.50$) were observed with regional meteorological data (Table 3), such as $\delta^{18}O$-Omega for BH and BR; $\delta^{18}O$-Precipitable water for BR and RC; $\delta^{18}O$-OLR only for BR; $\delta^{18}O$-Mix depth along HYSPLIT trajectories for BR and RC; the accumulated rainfall along HYSPLIT trajectories presented greater $\delta^{18}O$-correlations for all localities (Table 3).

The *d*-excess values were associated with large temporal variability. However, *d*-excess values can be divided into two periods (Fig. 4g). Until December, a large range of values was observed in RC (4.0‰–24.5‰), BR (1.15‰–20.96‰), and BH (2.09‰–18.12‰), while from January 2017 to March 2017, the observed variability was smaller, as observed at RC (4.2‰–17.1‰) and BH (5.68‰–15.71‰), while BR presented a similar variation (2.94‰–22.72‰). Only Cv (0.60) in BH and local precipitation (0.64) for BR exhibited strong correlations with *d*-excess (Table 3).

5. Discussion

The isotopic composition of precipitation in central-southeastern Brazil can be associated with the different processes in the atmosphere operating at different timescales (monthly or daily). Evaluation of the monthly isotopic composition revealed that seasonality is a common rainfall denominator across the region. The depleted (enriched) values (Fig. 3c) occurred during the rainy (dry) season (Fig. 2), in agree-

Table 2. Correlations between precipitation isotopes and meteorological data.

	Precipitation			Temperature			Warm phase (ONI)			Cold phase (ONI)		
Locations	$\delta^{18}O$	δ^2H	*d*	$\delta^{18}O$	δ^2H	*d*	$\delta^{18}O$	δ^2H	*d*-excess	$\delta^{18}O$	δ^2H	*d*-excess
Brasília	**–0.60**	**–0.09**	–0.001	0.13	0.17	0.18	0.23	0.22	–0.07	0.10	0.01	0.12
Rio de Janeiro	**–0.45**	**–0.45**	–0.08	**–0.44**	**–0.55**	–0.07	0.02	0.05	–0.003	0.07	0.12	0.23
Belo Horizonte	**–0.49**	**–0.49**	**–0.23**	0.17	–0.14	–0.01	0.21	0.18	0.18	0.47	0.47	0.20
Rio Claro	**0.63**	**0.31**	–0.17	**–0.29**	**–0.31**	–0.03	0.24	0.27	–0.01	0.51	0.51	0.02

d = *d*–excess. Bolded values are significant (*p*–value < 0.05).

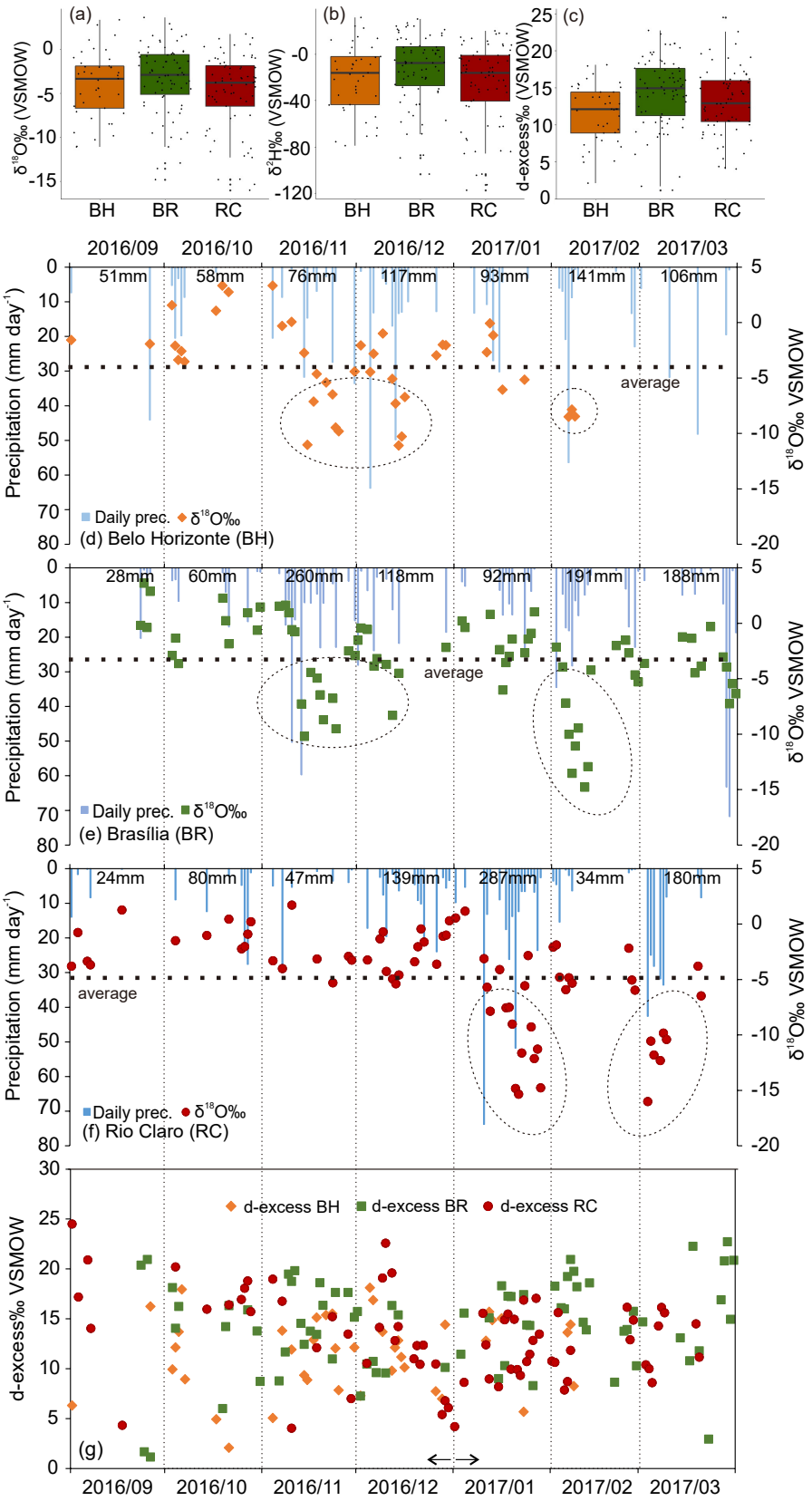

Fig. 4. Daily isotopic composition of precipitation at each site: (a) $\delta^{18}O$, (b) $\delta^{2}H$, and (c) *d*-excess dispersion boxplots; Blue bars represent the daily precipitation, dots $\delta^{18}O$ daily values for (d) BH, (e) BR, (f) RC, and (g) *d*-excess values for all sites. The average $\delta^{18}O$ value is represented by a dotted line, and depleted values are plotted below this line and indicated with blue circles. In (g) arrows indicate the two periods described in the text.

Table 3. Correlation between daily isotopic composition and meteorological data. Bolded values are significant (p-value < 0.05) and highlighted color in text are better correlations ($r > 0.50$).

Meteorological data		Belo Horizonte (BH)			Brasília (BR)			Rio Claro (RC)		
		$\delta^{18}O$	$\delta^{2}H$	d–excess	$\delta^{18}O$	$\delta^{2}H$	d–excess	$\delta^{18}O$	$\delta^{2}H$	d–excess
Local data	Precip.	**–0.20**	**–0.14**	**0.41**	**–0.39**	**–0.31**	**0.64**	**–0.30**	**–0.27**	**0.14**
	Temp.	0.02	0.00	–0.14	**0.27**	**0.24**	**–0.14**	**0.40**	**0.36**	**–0.20**
	RH	**–0.10**	**–0.10**	**0.05**	**–0.40**	**–0.36**	**0.22**	–0.16	–0.10	0.27
NOAA	OLR	**0.36**	**0.34**	**–0.23**	**0.57**	**0.55**	**–0.26**	**0.25**	**0.22**	**–0.12**
	Prec. Water	**–0.34**	**–0.32**	**0.17**	**–0.66**	**–0.65**	**0.23**	**–0.56**	**–0.59**	**–0.15**
	Omega	**0.65**	**0.61**	**–0.35**	**0.63**	**0.64**	**–0.14**	**0.36**	**0.32**	**–0.19**
ERA int.	Cv	**–0.35**	**–0.28**	**0.60**	**–0.34**	**–0.32**	**0.18**	**–0.30**	**–0.28**	**0.13**
	St	–0.07	–0.06	0.08	**–0.46**	**–0.44**	0.19	**–0.35**	**–0.32**	**0.20**
HYSPLIT model	Height	–0.07	–0.06	0.03	**0.18**	**0.13**	**–0.24**	**0.40**	**0.41**	**0.06**
	Pressure	0.12	0.10	–0.16	–0.04	0.01	0.13	**–0.36**	**–0.36**	**–0.01**
	Pot. Temp.	**–0.20**	**–0.17**	**0.24**	–0.05	–0.06	0.00	**0.29**	**0.29**	**–0.01**
	Amb. Temp.	–0.03	–0.03	0.06	**–0.13**	**–0.09**	**0.15**	**–0.39**	**–0.40**	**–0.05**
	Rainfall	**–0.57**	**–0.52**	**0.42**	**–0.58**	**–0.57**	**0.21**	**–0.56**	**–0.57**	**–0.09**
	Mix. depth	**0.49**	**0.43**	**–0.45**	**0.64**	**0.64**	**–0.26**	**0.49**	**0.51**	**0.16**
	RH	–0.13	–0.12	0.07	**–0.46**	–0.50	**0.09**	**–0.47**	**–0.51**	**–0.15**
	Terrain	–0.23	–0.16	0.56	**–0.22**	**–0.19**	**0.34**	–0.12	–0.12	–0.11
	Solar Rad.	0.06	0.07	0.04	**0.30**	**0.30**	**–0.07**	0.19	0.15	–0.19

ment with a previous study based on monthly timescales for RC (Gastmans et al., 2017; dos Santos et al., 2019a).

Monthly seasonality is not related to a temperature effect since there is a relatively small temperature seasonality between the warmer and colder months (highest value is 7° C) (Rozanski et al., 1993; Vuille et al., 2003; Jasechko, 2019). The lack of a temperature effect in tropical regions, where the temperature ranges from 20°C to 30°C, is often attributed to the dominance of the monthly amount effect (Rozanski et al., 1993) and the seasonal changes of the locations of storm origin.

The influence of ENSO did not result in significant differences in isotopic composition. Despite the existence of positive rainfall anomalies during the dry season (Fig. S1), there were no significant differences in historical rainfall rates or significant correlations between isotopic values and the ONI Index (Table 2). In fact, previous studies revealed that the central-southeastern region of Brazil is a transition region between the drier conditions to the north-northeast and wetter conditions over the southern portion of Brazil (Pezzi and Cavalcanti, 2001; Coelho et al., 2002; Barros et al., 2008; dos Santos et al., 2019b).

Greater average precipitation amounts were observed at BH and BR compared to RC and RJ, which may be associated with the SACZ position during the wet season (Zilli et al., 2019). Likewise, RC and RJ are the most often influenced by cold-frontal incursions during the dry season, which results in higher precipitation amounts compared to BH and BR. This trend may explain the differences between monthly isotopic compositions, such as the relative depletion in BH and enrichment in RJ, as well as the range of values (Fig. 3). In addition, the small isotope variability in RJ is associated with the proximity to the Atlantic Ocean, whereas in BR, the large variability is more related to the continental effect.

The distance to the Atlantic Ocean also affects moisture transport, highlighted by the LMWLs. Considering the monthly timescale, higher values of intercepts and slopes observed for BH and RC sites indicate that the isotopic composition of precipitation is influenced by the processes of moisture recirculation in the atmosphere (Wu et al., 2015; Tang et al., 2017; Putman et al., 2019).

Despite the short period of sampling, which covered most of the wet season over the region across all the sites, the observed daily isotopic composition is similar to the observed monthly data, with more enriched precipitation at BR compared to sampling period, which covered most of the wet season across all sites, the observed daily isotopic composition is similar to the observed monthly data, with more enriched precipitation observed at BR than BH and RC. The intercept of LMWLs for BH and RC sites showed lower values relative to the values derived from monthly data. According to Kurita et al. (2009), this is an expected trend because, on the monthly scale, the sum of rainfall events inhibits the local processes (post-condensation processes) that tend to decrease intercept values.

For this reason, the daily isotopic compositions (Fig. 4) are related to specific climatic features, acting over the region in different periods of the wet season. Contrary to those observed on a monthly timescale (Table 2), there was no amount effect observed on daily timescales (Table 3), and the most depleted values are not related to the larger precipitation events. During the wet season, both the radiation flux and temperatures are normally higher, which favor increased convective activity and the occurrence of large-scale SACZ events (Reboita et al., 2010).

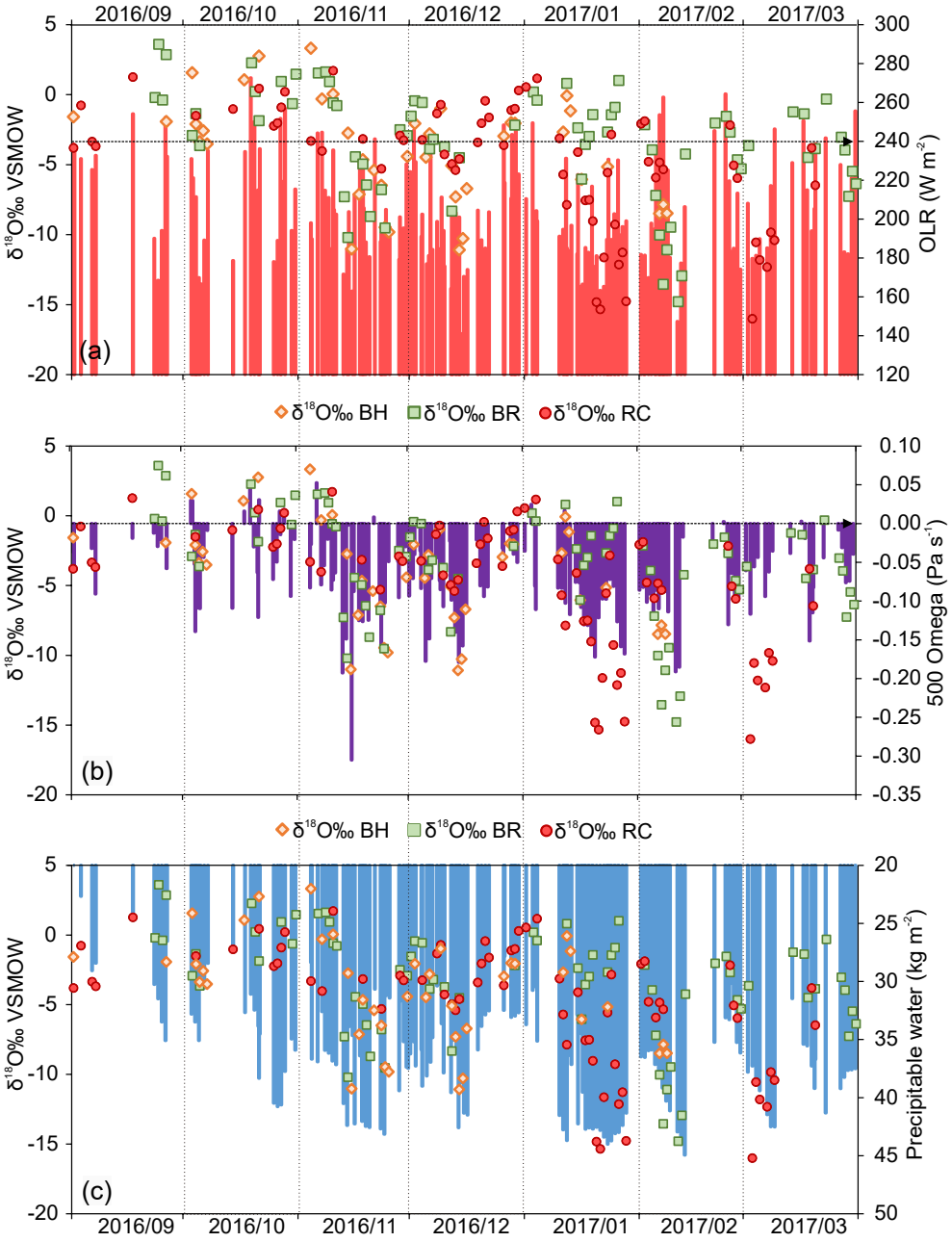

Fig. 5. Time series between $\delta^{18}O$ and NOAA meteorological data for all sites: (a) Outgoing Longwave Radiation (OLR, W m^{-2}); (b) Precipitable Water (kg m^{-2}); (c) Omega (Vertical velocity) at 500 hPa. Arrows indicate the limit of values associated with convective activity (< 240 W m^{-2} for OLR and negative for Omega).

Thereby, the differing displacements of daily isotopic variations (Fig. 4) are explained by convective activity (OLR < 240 W m^{-2} and negative values of Omega) and moisture contribution (HYSPLIT trajectories) (Fig. 6). The depleted $\delta^{18}O$ values (Fig. 5) in BH and BR were coupled with the lower OLR values between November-December (avg: 198 and 195 W m^{-2}, respectively), between February-March at BR (avg: 204 W m^{-2}), and between January (avg: 188 W m^{-2}) and March at RC (avg: 204 W m^{-2}) (Fig. 5a). Omega values (Fig. 5b) have similar distributions with OLR values, confirming the convective activity. This is evidenced by higher correlations between $\delta^{18}O$-OLR ($r > 0.55$; $p < 0.05$) and $\delta^{18}O$-Omega ($r > 0.61$; $p < 0\ .05$) (Table 3). Depleted $\delta^{18}O$ values were observed during negative peaks of omega values, representing a rising motion (Fig. 5b) and for low OLR values that occurred during the same period (Fig. 5a), while positive omega values were observed with enriched $\delta^{18}O$ values during September and early November (Fig. 5b), along with their associated higher OLR values (> 240 W m^{-2}) (Fig. 5a).

Large amounts of moisture in the atmosphere [high precipitable water values (PW)] were also observed during the

periods characterized by depleted $\delta^{18}O$ values and high convective activity (Fig. 5c). The first incursions of more depleted values in RC (Fig. 5c) were not observed before December (PW average between September-December: 32.18 kg m^{-2}) when an increase of the convective activity and PW occurred (PW avg during $\delta^{18}O$ depleted period in Fig. 5c: 41.59 kg m^{-2}). On the other hand, the first depleted incursions at BR and BH were observed in early November (Fig. 5c), associated with an early increase in PW and convective activity (Fig. 5). The observed differences indicate that regional climatic features are modulated in different ways at each site.

The temporal variability on moisture availability also impacts d-excess values, as indicated by the differences observed in the daily LMWL intercepts and the Kruskal-Wallis test. Thus, despite the constant increase in the availability of moisture in the atmosphere from September to December 2016, large variations in the PW values were observed for all locations: BH (19.23 kg m^{-2}–41.49 kg m^{-2}), BR (30.25 kg m^{-2}–43.14 kg m^{-2}), and RC (19.68 kg m^{-2}–40.77 kg m^{-2}). These large PW variations led to a greater variability for the observed *d*-excess values for this period (Fig. 4g). In contrast, from January to March, the PW variability was lower for BH (31.23 kg m^{-2}–39.54 kg m^{-2}) and RC (30.49 kg m^{-2}–44.94 kg m^{-2}), while BR was similar (30.49 kg m^{-2}– 44.94 kg m^{-2}), which led to lower observed variability in d-excess values (Fig. 4g).

Thereby, the large variability observed for PW and consequent d-excess values can be associated with different moisture sources and transport conditions that interact with atmospheric dynamics and regional circulation features, such as the LLJ (moisture transport from Amazon to central-south of Brazil) and the SASH (moisture transport from the Atlantic Ocean to central-south of Brazil). The trajectory maps display this difference between the sites with four moisture sources: land, ocean, and two with pathway over Amazon Forest (influenced by reevaporated moisture), originating from Land (named Land-Amazon; Fig. 6) or Ocean (Ocean-Amazon). The trajectories influenced by Amazon are accounted in the same percentage. Thus,. the trajectory contributions to the BH are 17% from the land and 83% from the ocean (9% influenced by Amazon Basin), for BR, 32% from the land and 68% from the ocean (22% from the Amazon Basin), and for RC 40% from the land and 60% from the ocean (21% from the Amazon basin) (Fig. 6).

Amazon moisture flux (Land-Amazon and Ocean-Amazon in Fig. 6a) traveled short distances to reach BR and, once associated with the SASH circulation (Ocean trajectories in Fig. 6a), they favor the moisture passage over BR (Fig. 6a), resulting in higher variations of PW and elevated *d*-excess values (avg: +14.40‰). On the other hand, the moisture from the Amazon (Land-Amazon and Ocean-Amazon; Fig. 6c) that reaches the RC site does experience larger transit distances. In addition, the site's association with cold-frontal activities (Ocean trajectories in the southern portion of map; Fig. 6c) produces a mixture of different moisture sources, resulting in lower *d*-excess values (avg: +13.09‰). Most of the moisture resulting in precipitation over BH originated from the Atlantic Ocean (Fig. 6b) and had a shorter pathway compared to the moisture arriving directly from the Atlantic Ocean to BR and RC; this is thought to have resulted in their lower *d*-excess values (avg: +11.55‰).

In addition, the higher correlations ($r \geq 0.50$) observed between $\delta^{18}O$ at the daily timescale and the regional parameters (Rainfall and Mix depth along HYSPLIT trajectories, PW, Omega, and OLR) (Table 3 and Fig. 5) confirm the importance of regional factors on governing isotope variations. They also reveal that seasonal effect related to the amount effect at a monthly timescale ($r \geq 0.60$ between $\delta^{18}O$-monthly precipitation) is explained by a combination of moisture sources, recirculation processes, and convective activity, better observed at a daily timescale.

Despite the relationship between $\delta^{18}O$ values and convective activity in RC, no statistical correlations were observed between $\delta^{18}O$ and OLR, Omega, and rainfall type by the ERA-interim. Thus, PW and Rainfall-HYSPLIT exhibited the best correlations, indicating that moisture availability is the key climate driver for RC, characterized by distinct moisture contributions and atmospheric systems, confirming the results demonstrated in previous studies (dos Santos et al., 2019a, c).

The effect of regional climatic characteristics was more evident in BR through correlations between $\delta^{18}O$ and regional meteorological parameters (Omega, OLR, PW, Rainfall-HYSPLIT, and Mix depth-HYSPLIT). The daily analysis confirmed the importance of the continental effect on a monthly scale, represented by a group of climatic features characterized by the interaction with convective activity, moisture transport, moisture source, and atmospheric systems (mainly the SACZ); thus, it is not possible to determine a single climatic driver for BR.

For BH, convective activity and moisture transport are important climatic features, confirmed by the strong correlation between Omega and Rainfall-HYSPLIT. The explanation for convective activity (movement of winds by atmospheric systems) is associated with SACZ and CF incursions, complemented by a weak correlation with $\delta^{18}O$ and OLR. The importance of air movement (convection or subsidence) during the formation of precipitation systems can be explained by the strong correlation between *d*-excess and Cv-Era in BH. These findings are coherent with previous assessments done by Risi et al. (2010), in which *d*-excess values were associated with processes of subsidence in the transition zones of convective-stratiform precipitation. However, few discussions have involved *d*-excess values and rainfall type due to the inherent difficulty in associating meteorological parameters with *d*-excess variability.

One possible explanation for weak correlations between daily $\delta^{18}O$-$\delta^{2}H$ and Cv-St precipitation is the sampling frequency and monitoring design since the classifications by Aggarwal et al. (2016) were specific to monthly data. The monthly $\delta^{18}O$ may be biased because the precipita-

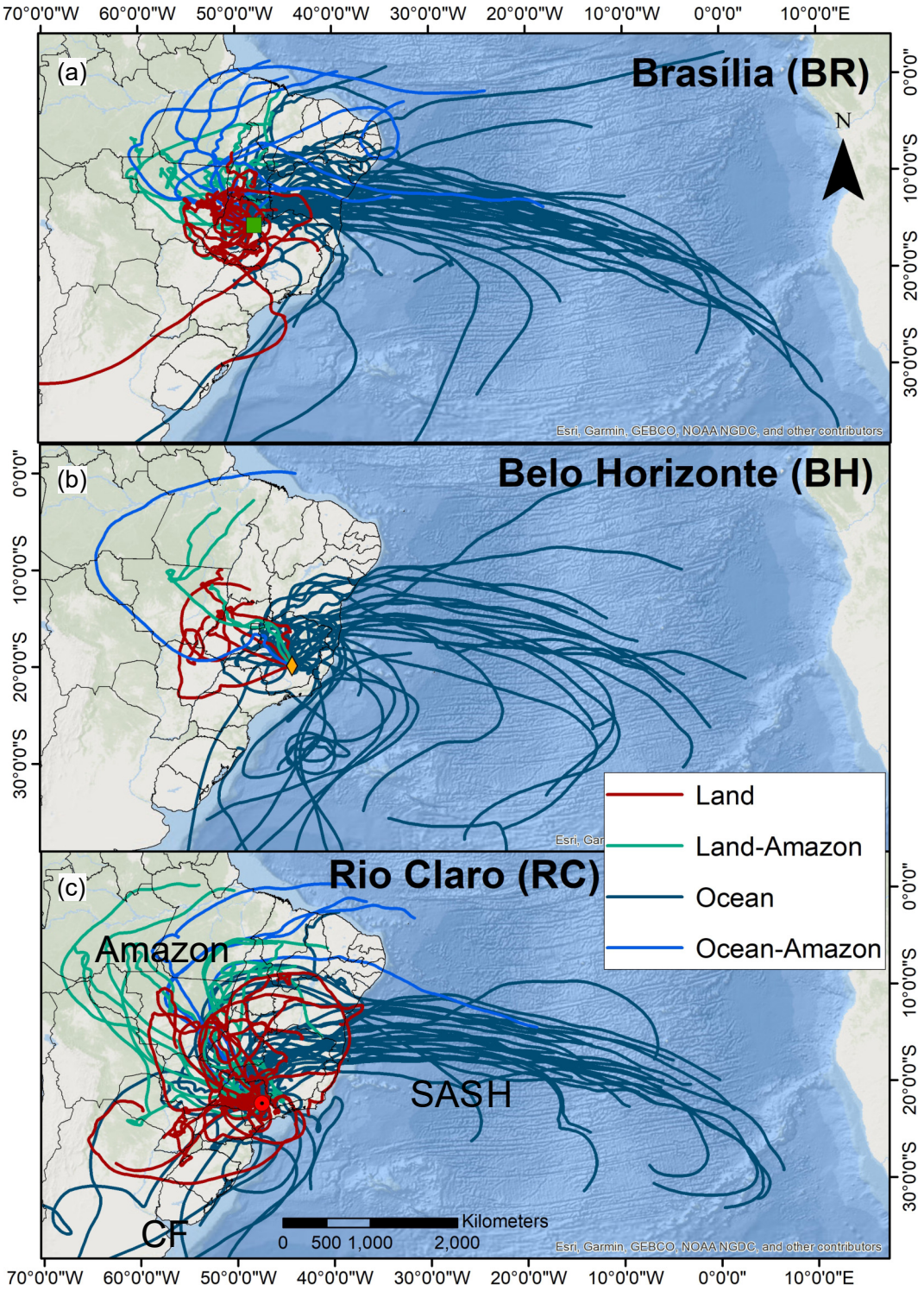

Fig. 6. Times series between $\delta^{18}O$ and NOAA meteorological data for all sites: (a) Outgoing Longwave Radiation (OLR, W m^{-2}); (b) Precipitable Water (kg m^{-2}); (c) Omega (vertical velocity) at 500 hPa. Arrows indicate the limit of values to convective activity (< 240 W m^{-2} for OLR and negative for Omega).

tion amount (P) also tends to increase with higher stratiform rain fraction, as mentioned by Konecky et al. (2019), such that the roles of moisture convergence and microphysical processes like rain re-evaporation (which also increases with P) remain hidden variables, mainly on monthly scales. The biased P was represented by similar distributions between daily $\delta^{18}O$-local precipitation (Fig. 4) and $\delta^{18}O$-Cv precipitation (Fig. S3), which also occurred with their correlations (Table 3). In addition, the daily data from RC was excluded from the convective/stratiform classification data using

Global Precipitation Measurement (GPM) by Munksgaard et al. (2019) due to weak correlation.

Moreover, SACZ and CF are responsible for organizing the convective activity over Brazil, generating precipitation systems formed by convective and stratiform precipitation (Machado and Rossow, 1993; Romatschke and Houze, 2013). These precipitation systems are estimated to be 45% convective and 46% stratiform in South America, noting that rainfall type is also difficult to partition (Romatschke and Houze, 2013).

Therefore, a combination of convective activity and moisture availability to the formation of precipitation systems agrees with other studies (Kurita et al., 2011; Kurita, 2013; Torri et al., 2017; Lacour et al., 2018) that demonstrate the major importance of climatic mechanisms, such as convection in relation to cloud microphysics (Aggarwal et al., 2016).

Our results demonstrate a relevant application of the role of convective activity on the isotopic variability of daily precipitation as a response to the interaction between moisture-convection, advancing the understanding of isotopic depletion and its poor correlation with the amount effect. However, it also highlights the strong relationship with δ^{18}O-OLR, as shown by Vuille and Werner (2005). Furthermore, it complements the assessment conducted by Kurita et al. (2011) and Lacour et al. (2018), whose focus was an assessment of the convection and isotopic composition of vapor and its response to precipitation. The spatial distribution of convection in locations over the continent differs from the regions over the tropical oceans (Torri et al., 2017) and those over a moisture convergence zone. The latter features intense convective activity, heavy rainfall, and large spatial distribution, such as the SACZ, which is generally used to explain the depleted isotopic composition of precipitation over the Americas (Gastmans et al., 2017; dos Santos et al., 2019c; Santos et al., 2021).

6. Conclusion

Sampling precipitation assessments of different timescales indicate how the different climatic features affect the isotopic composition of precipitation. While it was possible to visualize the isotopic variability associated with classic effects (seasonal, precipitation amount, and continentality) at the monthly scale, the daily isotopic composition revealed stronger relations to specific climatic features, such as convective activity and moisture transport.

Therefore, the variability observed at the daily scale was very helpful to understand how the available moisture interacts with the convective activity resulting in depleted δ^{18}O incursions, which are observed frequently during the wet season at different days at each site, and how the superposition of several events associated with these processes can result in monthly-scale depleted precipitation, leading to similar monthly seasonal variations for all sites, as well as for ENSO effects.

The observed differences in *d*-excess values, even on a monthly and daily basis, confirm the importance of recirculation processes that are governed by different moisture sources (the Atlantic Ocean and Amazon Forest) and pathways (modulated by the dynamics of atmospheric systems), resulting in depleted δ^{18}O values and large variability of *d*-excess values.

Thus, to quantify and improve the knowledge of tropical climate dynamics in the central-southeastern region of Brazil, there is a need to investigate the climatic (mechanisms) related to convection and the processes responsible for rainfall type (convective vs. stratiform) formation with the most robust meteorological data, such as radar or satellite products with enhanced resolutions, and intra-event collection of isotopic composition precipitation to investigate events related to the SACZ and CF.

Our results provide insights for new isotopic interpretation within the central-southeastern region of Brazil. Finally, our study may help to explain the hydrometeorological processes in a tropical region that is highly dependent on rainfall for hydroelectric power generation and agricultural production.

Acknowledgements. This work was funded by grants from the São Paulo Research Foundation (FAPESP) under Process 2018 /06666-4, and by the International Atomic Energy Agency grant BRA-17984 under the initiative CRP-F31004"Stable isotopes in precipitation and paleoclimatic archives in tropical areas to improve regional hydrological and climatic impact models ", and BRA-23531 under the initiative CRP-F31006 "Isotope Variability of Rain for Assessing Climate Change Impacts". VS thanks FAPESP for the scholarship provided under the Process 2019/03467-3. We would also like to thank Ling ZHOU and Xiayu YUAN , editors of the Advances in Atmospheric Sciences and two anonymous reviewers for their comments that have improved the initial manuscript.

Electronic supplementary material: Supplementary material is available in the online version of this article at https//doi.org/10.1007/s00376-022-1367-0.

REFERENCES

Aggarwal, P. K., O. A. Alduchov, K. O. Froehlich, L. J. Araguas-Araguas, N. C. Sturchio, and N. Kurita, 2012: Stable isotopes in global precipitation: A unified interpretation based on atmospheric moisture residence time. Geophys. Res. Lett., **39**, L11705, https://doi.org/10.1029/2012GL051937.

Aggarwal, P. K., U. Romatschke, L. Araguas-Araguas, D. Belachew, F. J. Longstaffe, P. Berg, C. Schumacher, and A. Funk, 2016: Proportions of convective and stratiform precipitation revealed in water isotope ratios. Nature Geoscience, **9**, 624–629, https://doi.org/10.1038/ngeo2739.

Alvares, C. A., J. L. Stape, P. C. Sentelhas, J. L. de Moraes Gonçalves, and G. Sparovek, 2013: Köppen's climate classification map for Brazil. Meteor. Z., **22**, 711–728, https://doi.org/10.1127/0941-2948/2013/0507.

Barros, V. R., M. E. Doyle, and I. A. Camilloni, 2008: Precipitation trends in southeastern South America: Relationship with ENSO phases and with low-level circulation. Theor. Appl. Cli-

matol., **93**, 19–33, https://doi.org/10.1007/s00704-007-0329-x.

Batista, L. V., D. Gastmans, R. Sánchez-Murillo, B. S. Farinha, S. M. R. dos Santos, and C. H. Kiang, 2018: Groundwater and surface water connectivity within the recharge area of Guarani aquifer system during El Niño 2014–2016. Hydrological Processes, **32**, 2483–2495, https://doi.org/10.1002/hyp.13211.

Berrisford, P., and Coauthors, 2011: The ERA-interim archive version 2.0. ERA Report Series No.1, 23 pp.

Bowen, G. J., Z. Y. Cai, R. P. Fiorella, and A. L. Putman, 2019: Isotopes in the water cycle: Regional- to global-scale patterns and applications. Annual Review of Earth and Planetary Sciences, **47**, 453–479, https://doi.org/10.1146/annurev-earth-053018-060220.

Clark, I., and P. Fritz, 1997: Environmental Isotopes in Hydrogeology. CRC Press, 342 pp.

Coelho, C. A. S., C. B. Uvo, and T. Ambrizzi, 2002: Exploring the impacts of the tropical Pacific SST on the precipitation patterns over South America during ENSO periods. Theor. Appl. Climatol., **71**, 185–197, https://doi.org/10.1007/s007040200004.

D'Agostino, R. B., A. Belanger, and R. B. D'Agostino Jr., 1990: A suggestion for using powerful and informative tests of normality. The American Statistician, **44**, 316–321, https://doi.org/10.1080/00031305.1990.10475751.

Dansgaard, W., 1964: Stable isotopes in precipitation. Tellus, **16**, 436–468, https://doi.org/10.3402/tellusa.v16i4.8993.

de Leeuw, J., J. Methven, and M. Blackburn, 2015: Evaluation of ERA-Interim reanalysis precipitation products using England and Wales observations. Quart. J. Roy. Meteor. Soc., **141**, 798–806, https://doi.org/10.1002/qj.2395.

dos Santos, V., D. Gastmans, L. V. Santarosa, L. V. Batista, S. B. Betancur, M. E. D. De Oliverira, and A. J. P. Filho, 2019a: Variabilidade da composição isotópica da precipitação na região central do estado de São Paulo. Revista Águas Subterrâneas, **33**, 171–181, https://doi.org/10.14295/ras.v33i2.29474.

dos Santos, V., M. D. de Oliveira, J. Boll, R. Sánchez-Murillo, A. A. Menegário, L. F. Gozzo, and D. Gastmans, 2019b: Isotopic composition of precipitation during strong El Niño–southern Oscillation events in the Southeast Region of Brazil. Hydrological Processes, **33**, 647–660, https://doi.org/10.1002/hyp.13351.

dos Santos, V., D. Gastmans, R. Sánchez-Murillo, L. F. Gozzo, L. V. Batista, R. L. Manzione, and J. Martinez, 2019c: Regional atmospheric dynamics govern interannual and seasonal stable isotope composition in southeastern Brazil. J. Hydrol., **579**, 124136, https://doi.org/10.1016/j.jhydrol.2019.124136.

Draxler, R., B. Stunder, G. Rolph, A. Stein, and A. Taylor, 2020: HYSPLIT USER's GUIDE. NOAA Version 5——Last Revision April, 2020. 249 pp. [Available online from https://www.arl.noaa.gov/documents/reports/hysplit_user_guide.pdf]

Ferreira, W. P. M., M. A. V. Silva and C. de F. Souza, 2018: Clima, recursos hídricos e produção agrícola: Perspectivas, desafios e possibilidades para a gestão. Informe Agropecuário, **39**, 65–79. (in Portuguese)

Gadgil, S., 2003: The Indian monsoon and its variability. Annual Review of Earth and Planetary Sciences, **31**, 429–467, https://doi.org/10.1146/annurev.earth.31.100901.141251.

Gastmans, D., V. Santos, J. A. Galhardi, J. F. Gromboni, L. V. Batista, K. Miotlinski, H. K. Chang, and J. S. Govone, 2017: Controls over spatial and seasonal variations on isotopic composition of the precipitation along the central and eastern portion of Brazil. Isotopes in Environmental and Health Studies, **53**, 518–538, https://doi.org/10.1080/10256016.2017.1305376.

Gimeno, L., A. Drumond, R. Nieto, R. M. Trigo, and A. Stohl, 2010: On the origin of continental precipitation. Geophys. Res. Lett., **37**, L13804, https://doi.org/10.1029/2010GL043712.

Gimeno, L., and Coauthors, 2021. The residence time of water vapour in the atmosphere. Nature Reviews Earth & Environment, **2**, 558–569, https://doi.org/10.1038/s43017-021-00181-9.

Graf, P., H. Wernli, S. Pfahl, and H. Sodemann, 2019: A new interpretative framework for below-cloud effects on stable water isotopes in vapour and rain. Atmospheric Chemistry and Physics, **19**, 747–765, https://doi.org/10.5194/acp-19-747-2019.

Han, T. T., M. J. Zhang, S. J. Wang, D. Y. Qu, and Q. Q. Du, 2020: Sub-hourly variability of stable isotopes in precipitation in the marginal zone of East Asian monsoon. Water, **12**, 2145, https://doi.org/10.3390/W12082145.

Han, X. K., and Coauthors, 2021: Temporal and spatial variations in stable isotopic compositions of precipitation during the typhoon Lekima (2019), China. Science of the Total Environment, **762**, 143143, https://doi.org/10.1016/j.scitotenv.2020.143143.

Huang, B. Y., and Coauthors, 2017: Extended reconstructed sea surface temperature, Version 5 (ERSSTv5): Upgrades, validations, and intercomparisons. J. Climate, **30**, 8179–8205, https://doi.org/10.1175/JCLI-D-16-0836.1.

Jasechko, S., 2019: Global isotope hydrogeology-review. Rev. Geophys., **57**, 835–965, https://doi.org/10.1029/2018RG000627.

Kalnay, E., and Coauthors, 1996: The NCEP/NCAR 40-year reanalysis project. Bull. Amer. Meteor. Soc., **77**, 437–472, https://doi.org/10.1175/1520-0477(1996)077<0437:TNYRP>2.0.CO;2.

Kirchheim, R. E., D. Gastmans, H. K. Chang, and T. E. Gilmore, 2019: The use of isotopes in evolving groundwater circulation models of regional continental aquifers: The case of the Guarani Aquifer System. Hydrological Processes, **33**, 2266–2278, https://doi.org/10.1002/hyp.13476.

Kodama, Y., 1992: Large-scale common features of subtropical precipitation zones (the Baiu Frontal Zone, the SPCZ, and the SACZ) Part I: Characteristics of subtropical frontal zones. J. Meteor. Soc. Japan, **70**, 813–836, https://doi.org/10.2151/jmsj1965.70.4_813.

Konecky, B. L., D. C. Noone, and K. M. Cobb, 2019: The influence of competing hydroclimate processes on stable isotope ratios in tropical rainfall. Geophys. Res. Lett., **46**, 1622–1633, https://doi.org/10.1029/2018GL080188.

Kruskal, W. H., and W. A. Wallis, 1952: Use of ranks in one-criterion variance analysis. Journal of the American Statistical Association, **47**, 583–621, https://doi.org/10.1080/01621459.1952.10483441.

Kurita, N., 2013: Water isotopic variability in response to mesoscale convective system over the tropical ocean. J. Geophys. Res., **118**, 10 376–10 390, https://doi.org/10.1002/jgrd.50754.

Kurita, N., K. Ichiyanagi, J. Matsumoto, M. D. Yamanaka, and T. Ohata, 2009: The relationship between the isotopic content of precipitation and the precipitation amount in tropical regions. Journal of Geochemical Exploration, **102**, 113–122, https://doi.org/10.1016/j.gexplo.2009.03.002.

Kurita, N., D. Noone, C. Risi, G. A. Schmidt, H. Yamada, and K. Yoneyama, 2011: Intraseasonal isotopic variation associated with the Madden-Julian Oscillation. J. Geophys. Res., **116**, D24101, https://doi.org/10.1029/2010JD015209.

Lacour, J.-L., C. Risi, J. Worden, C. Clerbaux, and P.-F. Coheur, 2018: Importance of depth and intensity of convection on the isotopic composition of water vapor as seen from IASI and TES δD observations. Earth and Planetary Science Letters, **481**, 387–394, https://doi.org/10.1016/j.epsl.2017.10.048.

Lekshmy, P. R., M. Midhun, and R. Ramesh, 2018: Influence of stratiform clouds on δD and $\delta^{18}O$ of monsoon water vapour and rain at two tropical coastal stations. J. Hydrol., **563**, 354–362, https://doi.org/10.1016/j.jhydrol.2018.06.001.

Lima, K. C., P. Satyamurty, and J. P. R. Fernández, 2010: Large-scale atmospheric conditions associated with heavy rainfall episodes in Southeast Brazil. Theor. Appl. Climatol., **101**, 121–135, https://doi.org/10.1007/s00704-009-0207-9.

Machado, L. A. T., and W. B. Rossow, 1993: Structural characteristics and radiative properties of tropical cloud clusters. Mon. Wea. Rev., **121**, 3234–3260, https://doi.org/10.1175/1520-0493(1993)121<3234:SCARPO>2.0.CO;2.

Marengo, J. A., W. R. Soares, C. Saulo, and M. Nicolini, 2004: Climatology of the low-level jet east of the Andes as derived from the NCEP-NCAR reanalyses: Characteristics and temporal variability. J. Climate, **17**, 2261–2280, https://doi.org/10.1175/1520-0442(2004)017<2261:COTLJE>2.0.CO;2.

Marengo, J. A., and Coauthors, 2012: Recent developments on the South American monsoon system. International Journal of Climatology, **32**, 1–21, https://doi.org/10.1002/joc.2254.

Michelsen, N., R. van Geldern, Y. Roßmann, I. Bauer, S. Schulz, J. A. C. Barth, and C. Schüth, 2018: Comparison of precipitation collectors used in isotope hydrology. Chemical Geology, **488**, 171–179, https://doi.org/10.1016/j.chemgeo.2018.04.032.

Michelsen, N., G. Laube, J. Friesen, S. M. Weise, A. B. A. B. Said, and T. Müller, 2019: Technical note: A microcontroller-based automatic rain sampler for stable isotope studies. Hydrology and Earth System Sciences, **23**, 2637–2645, https://doi.org/10.5194/hess-23-2637-2019.

Montini, T. L., C. Jones, and L. M. V. Carvalho, 2019: The South American low-level jet: A new climatology, variability, and changes. J. Geophys. Res., **124**, 1200–1218, https://doi.org/10.1029/2018JD029634.

Muller, C. L., A. Baker, I. J. Fairchild, C. Kidd, and I. Boomer, 2015: Intra-event trends in stable isotopes: Exploring midlatitude precipitation using a vertically pointing micro rain radar. Journal of Hydrometeorology, **16**, 194–213, https://doi.org/10.1175/JHM-D-14-0038.1.

Munksgaard, N. C., and Coauthors, 2019: Data Descriptor: Daily observations of stable isotope ratios of rainfall in the tropics. Scientific Reports, **9**, 14419, https://doi.org/10.1038/s41598-019-50973-9.

Pezzi, L. P., and I. F. A. Cavalcanti, 2001: The relative importance of ENSO and tropical Atlantic sea surface temperature anomalies for seasonal precipitation over South America: A numerical study. Climate Dyn., **17**, 205–212, https://doi.org/10.1007/s003820000104.

Power, S. B., F. P. D. Delage, C. T. Y. Chung, H. Ye, and B. F. Murphy, 2017: Humans have already increased the risk of major disruptions to Pacific rainfall. Nature Communications, **8**, 14368, https://doi.org/10.1038/ncomms14368.

Putman, A. L., R. P. Fiorella, G. J. Bowen, and Z. Y. Cai, 2019: A global perspective on local meteoric water lines: Meta-analytic insight into fundamental controls and practical constraints. Water Resour. Res., **55**, 6896–6910, https://doi.org/10.1029/2019WR025181.

R Core Team, 2020: The R Project for for Statistical Computing. R Foundation for Statistical Computing, Vienna, Austria. [Available online at https://www.R-project.org/.]

Ramos, A. M., R. C. Blamey, I. Algarra, R. Nieto, L. Gimeno, R. Tomé, C. J. C. Reason, and R. M. Trigo, 2019: From Amazonia to southern Africa: Atmospheric moisture transport through low-level jets and atmospheric rivers. Annals of the New York Academy of Sciences, **1436**, 217–230, https://doi.org/10.1111/nyas.13960.

Reboita, M. S., M. A. Gan, R. P. da Rocha, and T. Ambrizzi, 2010: Regimes de precipitação na América do Sul: Uma revisão bibliográfica. Revista Brasileira de Meteorologia, **25**, 185–204, https://doi.org/10.1590/S0102-77862010000200004.

Risi, C., S. Bony, and F. Vimeux, 2008: Influence of convective processes on the isotopic composition ($\delta^{18}O$ and δD) of precipitation and water vapor in the tropics: 2. Physical interpretation of the amount effect. J. Geophys. Res., **113**, D19306, https://doi.org/10.1029/2008JD009943.

Risi, C., S. Bony, F. Vimeux, M. Chong, and L. Descroix, 2010: Evolution of the stable water isotopic composition of the rain sampled along sahelian squall lines. Quart. J. Roy. Meteor. Soc., **136**, 227–242, https://doi.org/10.1002/qj.485.

Rolph, G., A. Stein, and B. Stunder, 2017: Real-time environmental applications and display system: READY. Environmental Modelling & Software, **95**, 210–228, https://doi.org/10.1016/j.envsoft.2017.06.025.

Romatschke, U., and R. A. Houze, 2013: Characteristics of precipitating convective systems accounting for the summer rainfall of tropical and subtropical South America. Journal of Hydrometeorology, **14**, 25–46, https://doi.org/10.1175/JHM-D-12-060.1.

Rozanski, K., L. Araguás-Araguás, and R. Gonfiantini, 1993: Isotopic patterns in modern global precipitation. Climate Change in Continental Isotopic Records, Volume 78, P. K. Swart et al., Eds., American Geophysical Union, 1–36, https://doi.org/10.1029/GM078p0001.

Sánchez-Murillo, R., and Coauthors, 2016: Key drivers controlling stable isotope variations in daily precipitation of Costa Rica: Caribbean Sea versus Eastern Pacific Ocean moisture sources. Quaternary Science Reviews, **131**, 250–261, https://doi.org/10.1016/j.quascirev.2015.08.028.

Sánchez-Murillo, R., A. M. Durán-Quesada, C. Birkel, G. Esquivel-Hernández, and J. Boll, 2017: Tropical precipitation anomalies and d-excess evolution during El Niño 2014-16. Hydrological Processes, **31**, 956–967, https://doi.org/10.1002/hyp.11088.

Sánchez-Murillo, R., and Coauthors, 2019: Deciphering key processes controlling rainfall isotopic variability during extreme tropical cyclones. Nature Communications, **10**, 4321, https://doi.org/10.1038/s41467-019-12062-3.

Santarosa, L. V., D. Gastmans, R. Sánchez-Murillo, V. dos San-

tos, L. V. Batista, and S. B. Betancur, 2021: Stable isotopes reveal groundwater to river connectivity in a mesoscale subtropical watershed. Isotopes in Environmental and Health Studies, **57**, 236–253, https://doi.org/10.1080/10256016.2021.1877701.

Santos, C., R. Carneiro, C. Borges, D. Gastmans, and L. Borma, 2021: Isotopic composition of precipitation in a southeastern region of Brazil during the action of the South Atlantic convergence zone. Atmosphere, **12**, 418, https://doi.org/10.3390/atmos12040418.

Soderberg, K., S. P. Good, M. O'Connor, L. X. Wang, K. Ryan, and K. K. Caylor, 2013: Using atmospheric trajectories to model the isotopic composition of rainfall in central Kenya. Ecosphere, **4**, 33, https://doi.org/10.1890/ES12-00160.1.

Stein, A. F., R. R. Draxler, G. D. Rolph, B. J. B. Stunder, M. D. Cohen, and F. Ngan, 2015: NOAA's HYSPLIT atmospheric transport and dispersion modeling system. Bull. Amer. Meteor. Soc., **96**, 2059–2077, https://doi.org/10.1175/BAMS-D-14-00110.1.

Tang, Y., X. F. Song, Y. H. Zhang, D. M. Han, L. K. Ai, T. B. Zhao, and Y. J. Wang, 2017: Using stable isotopes to understand seasonal and interannual dynamics in moisture sources and atmospheric circulation in precipitation. Hydrological Processes, **31**, 4682–4692, https://doi.org/10.1002/hyp.11388.

Terzer, S., L. I. Wassenaar, L. J. Araguás-Araguás, and P. K. Aggarwal, 2013: Global isoscapes for $\delta^{18}O$ and $\delta^{2}H$ in precipitation: Improved prediction using regionalized climatic regression models. Hydrology and Earth System Sciences, **17**, 4713–4728, https://doi.org/10.5194/hess-17-4713-2013.

Tharammal, T., G. Bala, and D. Noone, 2017: Impact of deep convection on the isotopic amount effect in tropical precipitation. J. Geophys. Res., **122**, 1505–1523, https://doi.org/10.1002/2016JD025555.

Torres, R. R., D. M. Lapola, J. A. Marengo, and M. A. Lombardo, 2012: Socio-climatic hotspots in Brazil. Climatic Change, **115**, 597–609, https://doi.org/10.1007/s10584-012-0461-1.

Torri, G., D. Ma, and Z. M. Kuang, 2017: Stable water isotopes and large-scale vertical motions in the tropics. J. Geophys. Res., **122**, 3703–3717, https://doi.org/10.1002/2016JD026154.

van der Ent, R. J., and O. A. Tuinenburg, 2017: The residence time of water in the atmosphere revisited. Hydrology and Earth System Sciences, **21**, 779–790, https://doi.org/10.5194/hess-21-779-2017.

Vera, C., and Coauthors, 2006: Toward a unified view of the American monsoon systems. J. Climate, **19**, 4977–5000, https://doi.org/10.1175/JCLI3896.1.

Vuille, M., and M. Werner, 2005: Stable isotopes in precipitation recording South American summer monsoon and ENSO variability: observations and model results. Climate Dyn., **25**, 401–413, https://doi.org/10.1007/s00382-005-0049-9.

Vuille, M., R. S. Bradley, M. Werner, R. Healy, and F. Keimig, 2003: Modeling $\delta^{18}O$ in precipitation over the tropical Americas: 1. Interannual variability and climatic controls. J. Geophys. Res., **108**, 4174, https://doi.org/10.1029/2001JD002038.

Wasko, C., and A. Sharma, 2017: Continuous rainfall generation for a warmer climate using observed temperature sensitivities. J. Hydrol., **544**, 575–590, https://doi.org/10.1016/j.jhydrol.2016.12.002.

Winnick, M. J., C. P. Chamberlain, J. K. Caves, and J. M. Welker, 2014: Quantifying the isotopic 'continental effect'. Earth and Planetary Science Letters, **406**, 123–133, https://doi.org/10.1016/j.epsl.2014.09.005.

Wu, H. W., X. P. Zhang, X. Y. Li, G. Li, and Y. M. Huang, 2015: Seasonal variations of deuterium and oxygen-18 isotopes and their response to moisture source for precipitation events in the subtropical monsoon region. Hydrological Processes, **29**, 90–102, https://doi.org/10.1002/hyp.10132.

Zilli, M. T., L. M. V. Carvalho, and B. R. Lintner, 2019: The poleward shift of South Atlantic Convergence Zone in recent decades. Climate Dyn., **52**, 2545–2563, https://doi.org/10.1007/s00382-018-4277-1.